Disorder-Induced Magnetotransport Anomalies in Amorphous and Textured Co 1– x Si x Semimetal Thin Films

Alan Molinari, Federico Balduini, Lorenzo Rocchino, Rafal Wawrzyńczak, Marilyne Sousa, Holt Bui, Christian Lavoie, Vesna Stanic, Jean Jordan-Sweet, Marinus Hopstaken, et al.

ACS APPLIED ELECTRONIC MATERIALS

pubs.acs.org/acsaelm Article

Disorder-Induced Magnetotransport Anomalies in Amorphous and Textured $Co_{1-x}Si_x$ Semimetal Thin Films

Alan Molinari,* Federico Balduini, Lorenzo Rocchino, Rafał Wawrzyńczak, Marilyne Sousa, Holt Bui, Christian Lavoie, Vesna Stanic, Jean Jordan-Sweet, Marinus Hopstaken, Serguei Tchoumakov, Selma Franca, Johannes Gooth, Simone Fratini, Adolfo G. Grushin, Cezar Zota, Bernd Gotsmann, and Heinz Schmid*

Cite This: *ACS Appl. Electron. Mater.* 2023, 5, 2624−2637 Read Online

ACCESS | Metrics & More | Article Recommendations | Supporting Information

ABSTRACT: In recent times the chiral semimetal cobalt monosilicide (CoSi) has emerged as a prototypical, nearly ideal topological conductor hosting giant, topologically protected Fermi arcs. Exotic topological quantum properties have already been identified in CoSi bulk single crystals. However, CoSi is also known for being prone to intrinsic disorder and inhomogeneities, which, despite topological protection, risk jeopardizing its topological transport features. Alternatively, topology may be stabilized by disorder, suggesting the tantalizing possibility of an amorphous variant of a topological metal, yet to be discovered. In this respect, understanding how microstructure and stoichiometry affect magnetotransport properties is of pivotal importance, particularly in case of low-dimensional CoSi thin films and devices. Here we comprehensively investigate the magnetotransport and magnetic properties of ≈25 nm $Co_{1-x}Si_x$ thin films grown on a MgO substrate with controlled film microstructure (amorphous vs textured) and chemical composition ($0.40 < x < 0.60$). The resistivity of $Co_{1-x}Si_x$ thin films is nearly insensitive to the film microstructure and displays a progressive evolution from metallic-like ($d\rho_{xx}/dT > 0$) to semiconducting-like ($d\rho_{xx}/dT < 0$) regimes of conduction upon increasing the silicon content. A variety of anomalies in the magnetotransport properties, comprising for instance signatures consistent with quantum localization and electron−electron interactions, anomalous Hall and Kondo effects, and the occurrence of magnetic exchange interactions, are attributable to the prominent influence of intrinsic structural and chemical disorder. Our systematic survey brings to attention the complexity and the challenges involved in the prospective exploitation of the topological chiral semimetal CoSi in nanoscale thin films and devices.

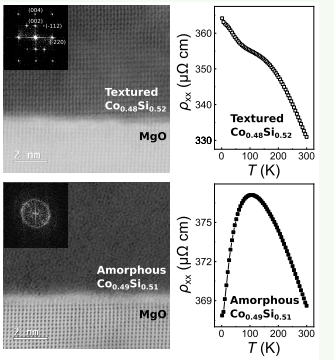

KEYWORDS: *CoSi, topological semimetals, amorphous thin films, magnetotransport, Hall effect*

INTRODUCTION

Topological materials, comprising for instance topological insulators, Dirac and Weyl semimetals, are characterized by exotic electronic band structures, which give rise to a variety of unconventional physical properties. The emergence of giant magnetoresistance, photogalvanic and thermoelectric effects,[1−6] the evidence for the violation of the Wiedemann−Franz law and the conservation of chirality,[4,7] and the presence of unusual quantum phenomena[8−10] make topological materials highly attractive for the exploration of novel device concepts in the areas of valleytronics,[11] quantum computing,[12] sensing,[3] and catalysis.[13]

Recently, novel types of chiral fermions—spin-1 and charge-2 fermions—as well as giant Fermi arcs traversing the entire surface Brillouin zone have been observed in the topological chiral semimetal CoSi.[14,15] In particular, the giant surface Fermi arcs of CoSi are orders of magnitude larger than those detected in the majority of chiral Weyl fermion semimetals. Besides, CoSi benefits from quasi-symmetry-protected topology, which makes it particularly resilient to perturbations such as strain-induced crystalline symmetry breaking.[16] The combination of these nontrivial topological properties highlights CoSi as a prospective, ideal topological conductor.

Experimental works on CoSi bulk single crystals have already shown a remarkable modulation in magnetoresistance (MR) up to 400% at 2 K and prominent quantum oscillations in both MR and thermoelectric signals.[17,18] However, CoSi is known for being sensitive to nonstoichiometries and disorder even in the case of bulk single crystals, which in turn provoke a marked variability in the magnetotransport and magnetic properties.[17,19,20]

Therefore, the question arises whether the topological properties of CoSi bulk single crystals survive in the case of

Received: January 22, 2023
Accepted: April 16, 2023
Published: April 25, 2023

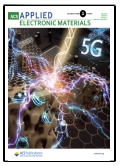

less-ideal, low-dimensional systems such as thin films[11,21,22] and nanowires,[23] which are required for nanoscale device applications. On the one hand, an increased surface-to-volume ratio should be beneficial for the exploitation of charge carrier transport along surface Fermi arcs, which, for instance, is envisioned as a promising route to overcome the resistivity bottleneck scaling of conventional metallic interconnects.[24−26] On the other hand, it is still unclear if low-dimensionality and structural and chemical disorder are compatible with topological magnetotransport.

Focusing on thin films, early works[21,27]—well before the discovery of the topological nature of CoSi—already pointed out the difficulties in stabilizing a pure cobalt monosilicide phase, owing to the tendency of formation of Co_2Si or $CoSi_2$ spurious phases, as also evidenced by the $Co_{1-x}Si_x$ phase diagram.[28] A careful control of the chemical composition in CoSi is also important since a variation in the Co content can trigger the formation of magnetic exchange interactions, which in turn affect the magnetotransport properties, particularly at low dimensionality. CoSi single crystals present rather weak diamagnetism with the possible onset of paramagnetism at temperatures below 25 K owing to the alignment of defect-generated paramagnetic centers in the presence of an external magnetic field.[19] Differently, unusual surface ferromagnetism and magnetic textures have been experimentally observed as the length scale of CoSi is brought to the nanoscale, such as in single-crystalline CoSi nanowires,[23,29] CoSi flakes,[30] and polycrystalline CoSi films above a critical cobalt excess of about 2.9%.[22] Besides, since band crossings typically realize Berry curvature monopoles in topological materials,[31] inserting controllably magnetic centers in CoSi may offer new opportunities to tailor its topological properties by breaking time-reversal symmetry.

The film microstructure represents another crucial parameter. Indeed, in topological materials crossing of linear bands in nontrivial nodal points or multifold degeneracies is stabilized by crystalline symmetries or quasi-symmetries.[16,32] In this respect, epitaxial CoSi films are desirable, for they are expected to better reflect the symmetry constraints, and in turn also the topological properties, of CoSi bulk single crystals. Yet, to date there has been no experimental realization of high-quality epitaxial CoSi thin films. Besides, from a device technological perspective, it is of interest to determine if topological protection may suffice to reveal signatures of topological transport in systems with large disorder, such as textured, polycrystalline or even amorphous CoSi thin films. Concerning the latter, a new research direction has recently sparked the search for possible exotic topological phases in amorphous systems, despite the absence of crystal symmetries.[33−35] Notably, amorphous topological metals have been predicted but remain undetected.[36]

In this work, we systematically investigate the influence of microstructure (amorphous vs textured) and chemical composition ($0.40 < x < 0.60$) on the magnetic and magnetotransport properties of $Co_{1-x}Si_x$ thin films with a thickness of ≈25 nm grown by molecular beam epitaxy (MBE) on (001)-oriented MgO substrates. The results show that the resistivity of amorphous $Co_{1-x}Si_x$ thin films is comparable to the one of textured $Co_{1-x}Si_x$ thin films. Furthermore, regardless of the very different microstructures, both amorphous and textured $Co_{1-x}Si_x$ thin films reveal an evolution from metallic-like ($d\rho_{xx}/dT > 0$) to semiconducting-like ($d\rho_{xx}/dT < 0$) regimes of conduction upon progressively increasing the silicon content. The prominent effects of disorder and inhomogeneities on the magnetotransport and magnetic properties are manifested in various ways. For instance Co-rich $Co_{1-x}Si_x$ thin films display enhanced magnetic interactions (ferromagnetic in textured films, superparamagnetic in amorphous films), as confirmed by pronounced magnetic hysteresis loops, butterfly-like MR, and anomalous Hall effect. The resistivity of amorphous Co-rich films exhibits an upturn at temperatures below 20 K, which can be explained in terms of the Kondo effect due to electron scattering with localized magnetic nanoparticles. We observe a transition from parabolic to quasi-linear MR in $Co_{1-x}Si_x$ thin films at temperatures below 50 K, which we attribute to disorder-induced quantum corrections potentially due to electron−electron interactions. Our results reveal the influence of structural and chemical disorder on the magnetotransport properties of low-dimensional $Co_{1-x}Si_x$ thin films, thus opening the path to the implementation of the prototypical topological chiral semimetal CoSi into future electronic and Weyltronic devices.

RESULTS AND DISCUSSION

Thin Film Growth and Characterization. A series of $Co_{1-x}Si_x$ thin films (thickness of about 25 nm) with finely tailored stoichiometry and microstructure were grown on (001)-oriented MgO substrates by the MBE method (see summary sketch in Figure 1). The chemical composition was varied in the $0.40 < x < 0.60$ range by carefully adjusting the fluxes of Co and Si electron-beam sources during a layer-by-layer MBE growth process; quantitative determination of the $Co_{1-x}Si_x$ films' stoichiometry was carried out by means of Rutherford backscattering spectroscopy (RBS). The growth temperature was found to be the main parameter affecting the microstructure of the $Co_{1-x}Si_x$ films with an amorphous-to-polycrystalline transition occurring at temperatures above the range of 100−175 °C, similarly to a previous work.[37] In the present study a maximum growth temperature of 360 °C was employed, because a substantial increase in surface roughness

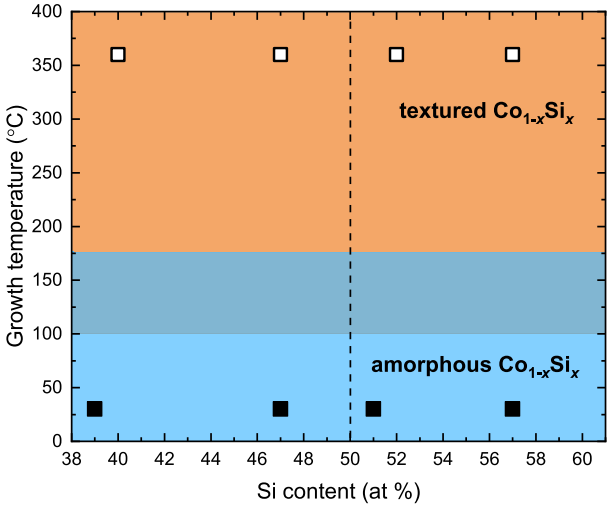

Figure 1. Diagram of the amorphous and textured $Co_{1-x}Si_x$ thin films fabricated by the MBE method with different chemical compositions and growth temperatures. Above (orange area) or below (light blue area) the temperature region of 100−175 °C the microstructure of the $Co_{1-x}Si_x$ film is predominantly amorphous or crystalline.

https://doi.org/10.1021/acsaelm.3c00095
ACS Appl. Electron. Mater. 2023, 5, 2624−2637

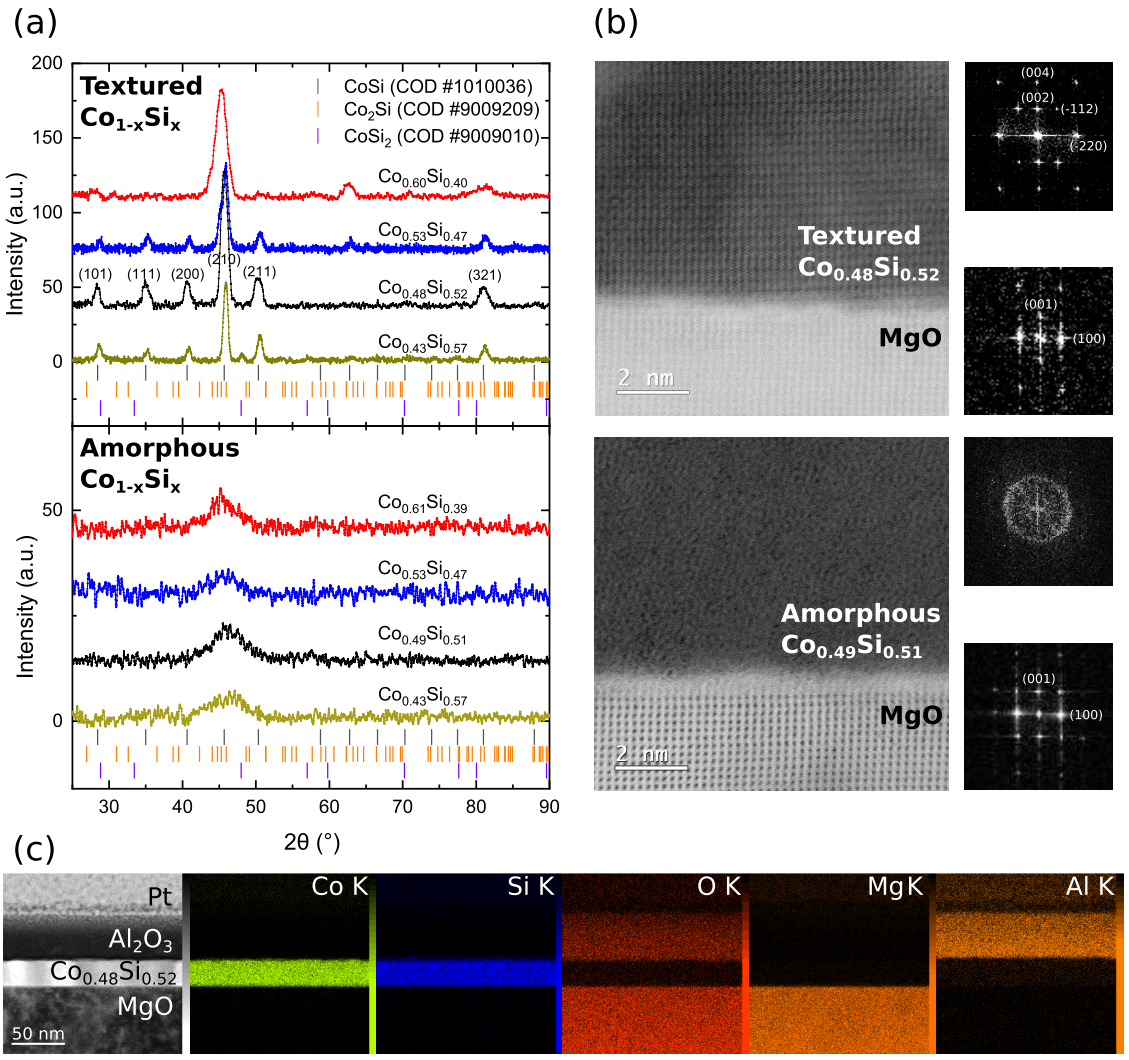

Figure 2. (a) Grazing-incident X-ray diffractograms of textured (top) and amorphous (bottom) $Co_{1-x}Si_x$ thin films with various compositions in the range $0.40 < x < 0.60$. Reference peaks of CoSi, Co_2Si, and $CoSi_2$ phases are taken from the crystallographic open database. (b) Bright-field, high-magnification scanning transmission electron micrographs of representative textured (top) and amorphous (bottom) $Co_{1-x}Si_x$ films close to 1-to-1 Co/Si ratio and respective fast Fourier transform patterns of the $Co_{1-x}Si_x$ films and the MgO substrate. (c) Dark-field, low-magnification scanning transmission electron micrograph of a textured $Co_{0.48}Si_{0.52}$ film revealing the presence of different grains with a lateral size of about 20−30 nm and related energy dispersive X-ray analysis showing a uniform distribution of Co and Si signals. The top Al_2O_3 film was used as protective layer.

due to island formation was observed upon increasing the growth temperature from 360 °C to 450 °C (see Figure S1).

Grazing-incident X-ray diffraction (GIXRD) analysis of the fabricated $Co_{1-x}Si_x$ samples reveals that all the films deposited at room temperature feature a broad and low-intensity peak in proximity to $2\theta \approx 45.9°$, which is the fingerprint of an amorphous microstructure with an average interatomic distance of 1.97 Å (Figure 2a bottom). As a comparison, the $Co_{1-x}Si_x$ films grown at a temperature of 360 °C have several sharp peaks, which are characteristic of a polycrystalline microstructure with an average domain size of about 10 nm, as calculated by the Scherrer formula (Figure 2a top).

Considering the $Co_{1-x}Si_x$ films grown at 360 °C, the X-ray peaks fit well with the reference CoSi reflections, thus suggesting that cobalt monosilicide is the predominant phase formed within the compositional range of $0.40 < x < 0.60$. This further suggests that in first approximation $Co_{1-x}Si_x$ can be treated as a solid-solution type alloy, although according to the bulk phase diagram[28] a deviation less than 2% from the ideal 1-to-1 Co/Si ratio is required in order to stabilize the cobalt monosilicide phase. Still, we underline that the vicinity of the reference CoSi peaks with reflections from other phases makes the interpretation of XRD results not always straightforward, in particular in the case of the $Co_{0.60}Si_{0.40}$ and $Co_{0.43}Si_{0.57}$ films grown at 360 °C (e.g., in the latter there is a small $CoSi_2$ peak at $2\theta \approx 48°$), which conspicuously deviate from the ideal 1-to-1 Co/Si ratio.

The results of GIXRD analysis and additional pole figure analysis carried out by means of synchrotron characterization reveal that the crystalline grains of the $Co_{1-x}Si_x$ films grown at 360 °C are not randomly oriented, but they rather present a pronounced in-plane and out-of-plane texture orientation with respect to the MgO substrate (more details in Figure S2).

The results of the XRD survey are supported by the scanning transmission electron microscopy (STEM) and fast Fourier transform (FFT) analyses of representative cross sections of nearly stoichiometric $Co_{1-x}Si_x$ films (see Figure 2b). The lack of long-range order and the blurred ring in the

https://doi.org/10.1021/acsaelm.3c00095
ACS Appl. Electron. Mater. 2023, 5, 2624−2637

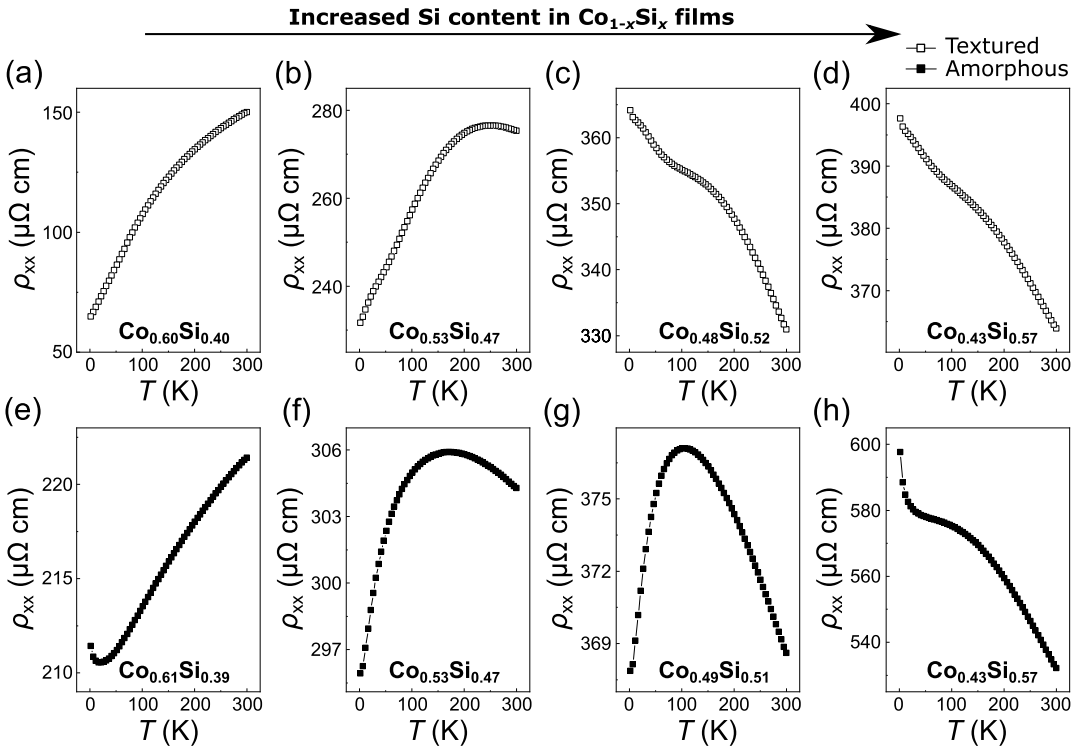

Figure 3. Temperature-dependent ρ_{xx} curves of textured (a−d) and amorphous (e−h) $Co_{1-x}Si_x$ films in the range of composition $0.40 < x < 0.60$. Upon increasing the Si content, the resistivity curves undergo a transition from metallic to semiconducting-like conduction regimes. The low-temperature upturn in the ρ_{xx} curves in (e) and (h) is attributed to the Kondo effect and electron−electron interactions, respectively.

STEM and FFT images of the $Co_{0.49}Si_{0.51}$ films grown at room temperature confirm an amorphous film microstructure. In contrast, the $Co_{0.48}Si_{0.52}$ sample grown at 360 °C displays a coherent stacking of the CoSi unit cells in proximity of the interface with the MgO substrate. The local interfacial area analyzed in Figure 2b (top) denotes an out-of-plane epitaxial relation between film and substrate given by CoSi (00l) || MgO (00l). The size of the $Co_{1-x}Si_x$ grains having a nearly epitaxial relation with the MgO substrate is on the order of 20−30 nm. Concerning the chemical composition, local inspection via energy dispersive X-ray analysis reveals a uniform distribution of Co and Si elements in the $Co_{0.48}Si_{0.52}$ film grown at 360 °C (see Figure 2c). The absence of oxygen or other elements overlapping with the Co and Si signals demonstrates the lack of film oxidation through the film thickness or interfacial interdiffusion, thus supporting the high quality of the fabricated films. As mentioned, the chemical composition of all the investigated $Co_{1-x}Si_x$ films has been quantitatively inspected by means of the RBS method; more details about sample preparation and characterization can be found in the Experimental Section and in Figures S3−S6.

Electrical Resistivity, Magnetoresistance, and Magnetization Measurements. We now analyze the electrical resistivity ρ_{xx} of amorphous and textured $Co_{1-x}Si_x$ films with $0.40 < x < 0.60$ in the temperature range of 2−300 K (see Figure 3). At room temperature the values of ρ_{xx} progressively increase in the range of 150−360 $\mu\Omega$ cm and 220−530 $\mu\Omega$ cm respectively for textured and amorphous $Co_{1-x}Si_x$ films upon substitution of Co with Si sites; in particular, in the case of the $Co_{1-x}Si_x$ samples approaching the ideal 1-to-1 CoSi stoichiometry, i.e., textured $Co_{0.48}Si_{0.52}$ in Figure 3c and amorphous $Co_{0.49}Si_{0.51}$ in Figure 3g, ρ_{xx} is on the order of 330−370 $\mu\Omega$ cm.

Considering the trend of the temperature-dependent curves, one can notice a systematic change of slope of $\rho_{xx}(T)$ upon increasing the silicon content. Textured and amorphous $Co_{1-x}Si_x$ films with about 10% Co excess $Co_{0.60}Si_{0.40}$ films display a monotonic decrease in ρ_{xx} as the temperature decreases, similarly to the behavior of conventional metals. Textured $Co_{0.60}Si_{0.40}$ films achieve the largest residual resistivity ratio (RRR) = $\rho_{xx}(300\ K)/\rho_{xx}(2\ K) \approx 2.3$, whereas all the other investigated $Co_{1-x}Si_x$ samples have an RRR close to unity. As the composition approaches $x \approx 0.5$, the temperature-dependent ρ_{xx} curves reveal a nonmonotonic behavior; in particular a characteristic plateau is formed in the temperature range of 120−250 K. Such plateau, which is commonly observed in semimetals[38] and narrow-gap semiconductors,[39] lies at higher or lower temperatures in relation to a slight excess of Co or Si, respectively. Then, at even higher values of silicon content $x \approx 0.57$ the amorphous and textured $Co_{1-x}Si_x$ films display a quasi-monotonic increase in resistivity as the temperature is decreased, similarly to the case of semiconductors or strongly disordered metals.

We note that the Co-rich and Si-rich amorphous $Co_{1-x}Si_x$ films, i.e., $Co_{0.61}Si_{0.39}$ in Figure 3e and $Co_{0.43}Si_{0.57}$ in Figure 3h, display some peculiar features not exhibited by the other samples; in particular, there is a distinct upturn in ρ_{xx} below 20−30 K followed by a logarithmic temperature dependence of ρ_{xx} down to 2 K (see also Figure S7). This behavior may be a consequence of the Kondo effect due to strong interaction of charge carriers with localized magnetic impurities,[20,40] or quantum corrections to electrical conduction due to weak localization,[19,41] or disorder-enhanced electron−electron interaction.[42] In 2D films these different mechanisms provide a similar logarithmic temperature-dependence of ρ_{xx}, thus making a distinction between them not trivial. The analysis

https://doi.org/10.1021/acsaelm.3c00095
ACS Appl. Electron. Mater. 2023, 5, 2624−2637

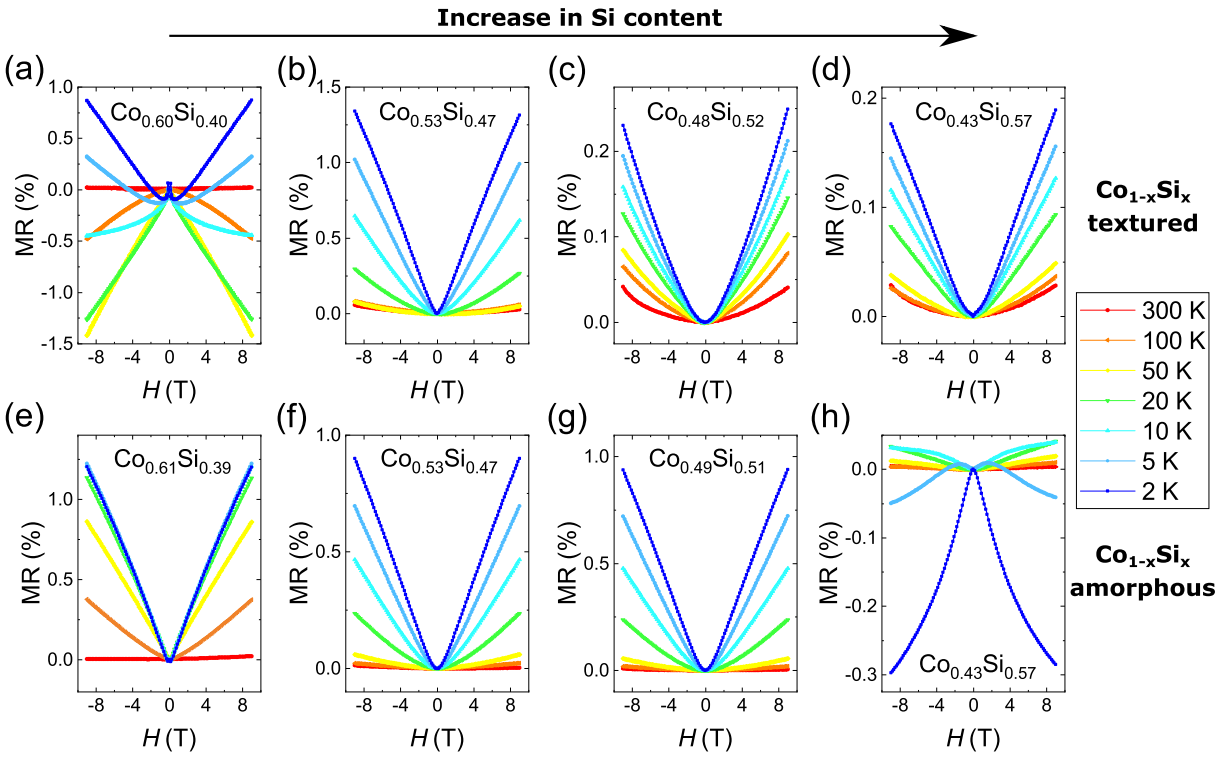

Figure 4. Transverse MR of textured (a–d) and amorphous (e–h) $Co_{1-x}Si_x$ films in the range of composition $0.40 < x < 0.60$ at different temperatures and applied magnetic fields. In all measurements the applied magnetic field is perpendicular to the current flow.

of MR and magnetization described in the following is helpful to disentangle the different phenomena.

Regardless of the various degrees of intrinsic structural order (and thus also of transport mechanisms), both textured and amorphous $Co_{1-x}Si_x$ films manifest a similar change of slope in the temperature-dependent ρ_{xx} curves. Typically, electrical transport in polycrystalline films is dominated at high temperature by scattering of the charge carriers with phonons and at low temperature by scattering with intrinsic defects, such as the sample surface, interfaces, and grain boundaries.[43] Differently, amorphous systems are characterized by intrinsic short-range structural order, which causes the carriers' mean free path to be on the order of the interatomic distance. In general, the charge carriers contributing to the electrical transport in amorphous systems can be distinguished in localized or extended states being separated in energy by a *mobility edge* or a *mobility gap*; the metallic/insulating character of the material is then determined by the position of the Fermi energy with respect to the localized region. In amorphous semiconductors, such as a-Si, localized states dominate and conduction typically occurs through a thermally induced, variable range hopping process, with a conductivity that follows the Mott[44] relation $\sigma \propto \exp(T^{-1/4})$ where T is the absolute temperature. The compounds under study, however, lie outside the domain of applicability of activated hopping since all exhibit a small overall change in resistance (less than a decade, and thus hardly attributable to an exponential). As the composition is varied, we observe a progressive reduction and change of sign of the slope of the temperature-dependent resistivity at room temperature, a phenomenology that is commonly observed in strongly disordered metals.[45,46] The resistivity curves indicate that the present samples exhibit so-called Mooij[45] correlations: $d\rho_{xx}/dT$ decreases linearly with the interpolated intercept ρ_0, changing sign at a value of ρ_0 that is comparable to the Mott–Ioffe–Regel value ρ_{MIR}, the latter defined as the resistivity of a metal where the carrier mean-free-path equals the lattice spacing (see Figure S8 and Table S1 for numerical values and in-depth analysis). Possible microscopic mechanisms that have been advanced to explain this behavior include quantum localization corrections[47] and polaron formation favored by disorder.[48] Highly relevant to the present compounds, this phenomenology also arises in disordered systems when the Fermi energy is tuned across a band edge, corroborating the semimetallic nature of the $Co_{1-x}Si_x$ films.[49] Remarkably, the band tuning scenario naturally implies sizable changes of the carrier density with composition x (see Hall measurements below) and leads to the emergence of resistivity maxima at intermediate temperatures,[49] both observed here.

To put our resistivity data into a broader context, we note that previous works report a room temperature $\rho_{xx} \approx 100-150$ $\mu\Omega$ cm for CoSi bulk single crystals[17,18] and $\rho_{xx} \approx 100-350$ $\mu\Omega$ cm for CoSi polycrystalline thin films.[11,21] First, we remark that the order of magnitude of ρ_{xx} of our $Co_{1-x}Si_x$ films is consistent with literature, though the value of nearly stoichiometric films appears to be slightly higher. Second, it is quite surprising that the values of ρ_{xx} are very similar in amorphous and textured $Co_{1-x}Si_x$ films and even comparable to some single-crystalline samples with low RRR.[17,18] This may be attributed to the fact that CoSi—even in the form of single crystals—belongs to the category of strongly disordered metals,[19] thus reflecting a situation where intrinsic defects and disorder heavily impact the electronic transport. Yet, it is well established that amorphous materials are typically much worse conductors than their crystalline counterparts.[44,50,51] We further discuss this aspect in connection to the values of mobilities and charge carrier concentration provided in the Hall effect analysis below.

https://doi.org/10.1021/acsaelm.3c00095
ACS Appl. Electron. Mater. 2023, 5, 2624–2637

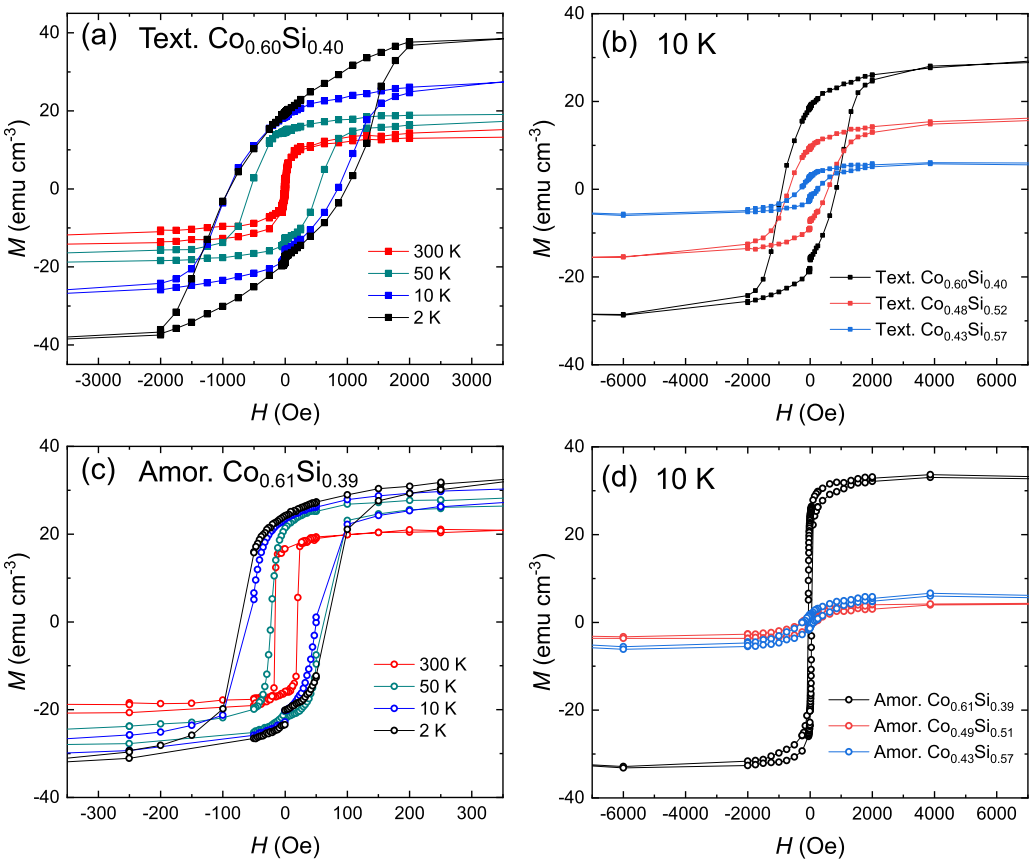

Figure 5. Analysis of the magnetization of $Co_{1-x}Si_x$ thin films as a function of the applied magnetic field. (a) $M(H)$ curves of a textured, Co-rich $Co_{0.60}Si_{0.40}$ film at different temperatures. (b) Comparison of $M(H)$ curves of textured $Co_{1-x}Si_x$ films with x = 0.40, 0.52, and 0.57 at 10 K. (c) $M(H)$ curves of amorphous, Co-rich $Co_{0.61}Si_{0.39}$ films at different temperatures. (d) Comparison of $M(H)$ curves of amorphous $Co_{1-x}Si_x$ films with x = 0.39, 0.51, and 0.57 at 10 K. The results in (a) and (c) are for $Co_{1-x}Si_x$ samples not characterized by RBS, but grown under the same MBE conditions as the ones characterized by RBS. In all measurements the applied magnetic field is parallel to the in-plane orientation of the $Co_{1-x}Si_x$ films.

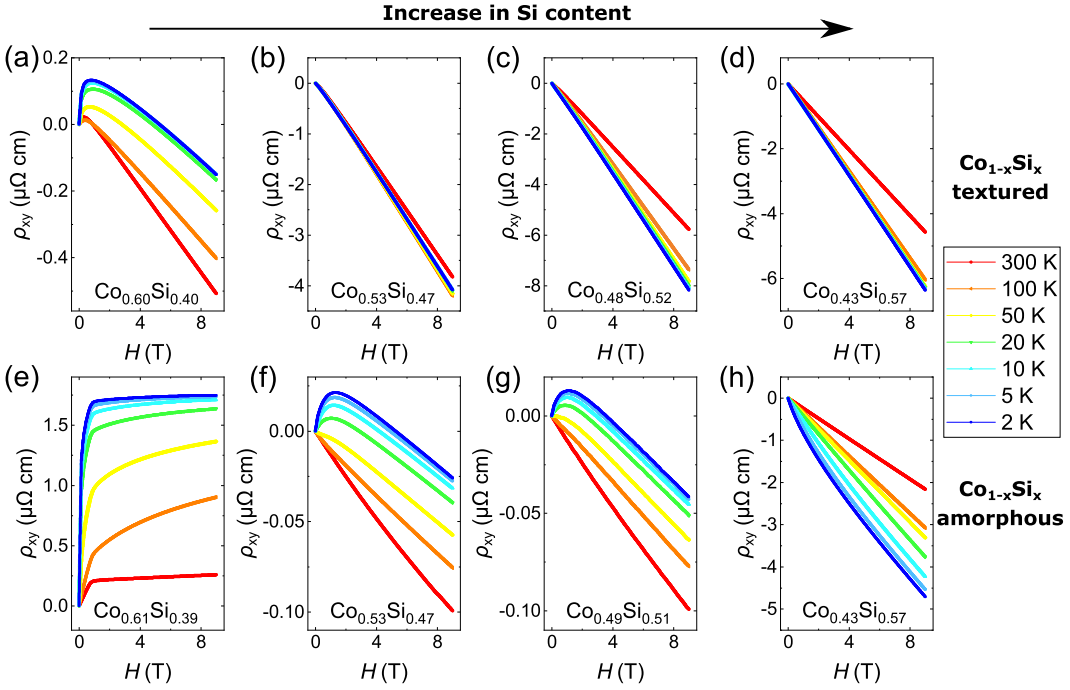

Figure 6. Antisymmetrized Hall resistivity of textured (a–d) and amorphous (e–h) $Co_{1-x}Si_x$ films in the range of composition 0.40 < x < 0.60 at different temperatures and applied magnetic fields. In all measurements the applied magnetic field is perpendicular to the current flow.

https://doi.org/10.1021/acsaelm.3c00095
ACS Appl. Electron. Mater. 2023, 5, 2624–2637

In order to gain deeper insights into the conduction mechanisms of $Co_{1-x}Si_x$ thin films, we have investigated the transverse MR (Figure 4), the magnetization (Figure 5), and the Hall effect (Figure 6) in the 2−300 K temperature range with applied magnetic fields up to ±9 T.

Textured $Co_{0.60}Si_{0.40}$ films present a negative transverse MR with a maximum variation of −1.5% upon decreasing the temperature from 300 K to 50 K. Below 50 K the transverse MR progressively turns from negative to positive and reaches a value of +1% at 2 K and high magnetic fields (see Figure 4a). The occurrence of negative transverse MR in the textured Co-rich $Co_{0.60}Si_{0.40}$ films already hints toward the possible presence of robust ferromagnetism. In textured $Co_{1-x}Si_x$ films with compositions x = 0.47, 0.52, and 0.57 the transverse MR is dominated by a positive response with a systematic decrease in its magnitude from 1.2% to 0.18% for increasing x (see Figure 4b−d). Concerning the amorphous $Co_{1-x}Si_x$ films, the samples with x = 0.39, 0.47, and 0.51 have a positive transverse MR with a modulation of about 1% (see Figure 4e−g). It is worth noticing that the amorphous Co-rich $Co_{0.61}Si_{0.39}$ film, unlike its textured Co-rich counterpart, does not present an evident sign of negative transverse MR, except for a small hint at 2 K and low magnetic fields (see also Figure S10).

The amorphous $Co_{0.43}Si_{0.57}$ film shows the most atypical transverse MR behavior, with an abrupt transition from positive to negative response below 5 K (see Figure 4h). As mentioned above, such amorphous Si-rich $Co_{0.43}Si_{0.57}$ sample is also the one displaying an unusual low-temperature upturn in ρ_{xx}. The behavior of ρ_{xx} and MR curves indicates the possible presence of localization effects or electron−electron interaction (EEI), similarly to the case of topological semimetal Cd_3As_2 films[41] and topological insulator Bi_2Se_3 films.[42] Localization effects can appear in the form of weak localization (WL) or weak antilocalization (WAL). WL (WAL) occurs due to the constructive (destructive) interference of electron wave functions with defects and impurities along a back scattering path in a quantum diffusive conduction regime.[52] WL (WAL) brings about an enhanced (diminished) probability of electron localization. A distinctive characteristic of WL (WAL) is that it gives rise to negative (positive) transverse MR[53] often accompanied by cusp-like features, which are suppressed as the magnetic field is increased.[41,54] Therefore, the sharp increase in ρ_{xx} at low temperature (see Figure 3h) and the negative transverse MR (see Figure 4h) in amorphous Si-rich $Co_{0.43}Si_{0.57}$ films point toward a possible contribution of a WL effect. The variation from positive to negative transverse MR upon decreasing temperature in the Si-rich $Co_{0.43}Si_{0.57}$ sample may indicate a transition from WAL to WL.[41,55] However, EEI can affect the magnetotransport properties in a similar manner to localization effects. EEI is triggered by enhanced Coulomb interactions between electrons in highly disordered metals. The origin of this anomaly is related to the fact that in disordered metals the electrons can only propagate by diffusion, and thus a sudden variation in charge distribution is screened with a certain delay.[55] In contrast to WL or WAL, EEI is much less sensitive to the orientation and magnitude of the applied magnetic fields.[56,57] In this sense, the isotropic character of transverse MR and longitudinal MR signals, whose curves can be nearly superimposed (see Figure S11), is compatible with an EEI scenario. In addition, WL and WAL are suppressed in the presence of large magnetic fields because of the destruction of electron phase coherence. In our case below 20 K the temperature-dependent ρ_{xx} curves of amorphous Si-rich $Co_{0.43}Si_{0.57}$ films in the presence and absence of an applied magnetic field of 9 T have a nearly perfect overlap (see Figure S12). This is a clear indication that the low-temperature quantum corrections to conductivity in amorphous Si-rich $Co_{0.43}Si_{0.57}$ films are dominated by EEI rather than one-body localization effects, though a small contribution of the latter cannot be completely excluded. We note that the concurrent presence of EEI and WL (or WAL) effects is not uncommon in amorphous and topological systems.[42,58,59] Moreover, we note that textured Si-rich $Co_{0.43}Si_{0.57}$ films reveal a small cusp-like feature at 2 K and low magnetic fields (see Figure 4d and Figure S9), which can be possibly attributed to WAL or EEI effects.

A closer inspection of the transverse MR curves permits to grasp further details. First, differently from the classical parabolic MR due to the contribution of the Lorentz force in metals and semimetals, the transverse MR curves of amorphous and textured $Co_{1-x}Si_x$ thin films undergo a transition from quadratic to nonsaturating, quasi-linear response upon increasing the magnetic field at temperatures below ≈50 K. This behavior is more clearly visualized in the derivatives of the transverse MR curves (see Figure S13), which present a crossover field B_L of about 1−2 T. Below we delve deeper into the possible phenomena that give rise to a transition from quadratic to quasi-linear MR in $Co_{1-x}Si_x$ thin films.

Second, by sweeping back and forth the direction of the magnetic field in the range of ±1.5 T, the transverse MR curves trace a butterfly-like shape (see the Figures S9, S10), which is especially pronounced for the films with higher Co concentration. Such butterfly-like shape is a fingerprint of the occurrence of magnetism in amorphous and textured $Co_{1-x}Si_x$ films.

Magnetic characterization (see Figure 5) confirms the presence of robust magnetic exchange interactions, whose strength is directly correlated to the amount and distribution of Co in amorphous and textured $Co_{1-x}Si_x$ films. Textured $Co_{0.60}Si_{0.40}$ films achieve the largest values of magnetization saturation, $M_s \approx 39$ emu/cm^3, and coercivity, $H_c \approx 1000$ Oe, whereas amorphous $Co_{0.61}Si_{0.39}$ films feature a comparable $M_s \approx 36$ emu/cm^3, but a markedly smaller $H_c \approx 100$ Oe. The other $Co_{1-x}Si_x$ thin films still display magnetic hysteresis loops with a tendency toward a lower M_s as the cobalt concentration is progressively decreased. The main influence of the microstructure is that textured $Co_{1-x}Si_x$ films have larger values of H_c as compared to the amorphous counterparts.

The analysis of the temperature-dependent magnetization ($M(T)$) (see Figure S14) reveals a net separation between zero field and field cooled (ZFC−FC) curves in textured $Co_{1-x}Si_x$ films with a maximum blocking temperature T_B of about 150 K for x = 0.40. Differently, in case of amorphous $Co_{1-x}Si_x$ films the ZFC−FC curves have a near perfect overlap onto each other.

Besides, we note that the $M(T)$ curves do not undergo any steep transition in the range of 2−300 K, thus suggesting that the Curie temperature (T_C) lies above room temperature. The steep increase in $M(T)$ occurring below 15 K is likely related to the contribution of paramagnetic impurities intrinsic in the bulk MgO substrate,[60] as also confirmed by the $M(T)$ measurement on a reference MgO substrate.

From the breadth of the $M(H)$ curves and the behavior of the ZFC−FC curves, it is inferred that textured $Co_{1-x}Si_x$ thin films include ferromagnetic nanoparticles in the micro-

https://doi.org/10.1021/acsaelm.3c00095
ACS Appl. Electron. Mater. 2023, 5, 2624−2637

structure, whereas amorphous $Co_{1-x}Si_x$ thin films comprise soft ferromagnetic particles close to the threshold of superparamagnetism.[61] The different ferromagnetic and near-superparamagnetic responses are likely ascribed to a different distribution of cobalt within the amorphous and textured microstructures as a consequence of the growth temperatures employed during MBE deposition. In a plausible scenario, textured $Co_{1-x}Si_x$ films deposited at a temperature of 360 °C experience an enhanced diffusion and nucleation of Co into larger magnetic clusters during the MBE growth process. In contrast, Co species are embedded more uniformly in the disordered lattice of amorphous $Co_{1-x}Si_x$ films grown at room temperature, thus forming smaller, isolated superparamagnetic nanoparticles. The tendency for the formation of Co-rich clusters with a size of several nanometers in textured $Co_{0.60}Si_{0.40}$ films is confirmed by the EDX analysis (see Figure S5); such clusters could not be detected in the case of nearly stoichiometric $Co_{1-x}Si_x$ thin films (see Figure 2c). The presence of Co-rich clusters with different size and distribution in amorphous and textured $Co_{1-x}Si_x$ films may also explain some of the apparent anomalies observed in the ρ_{xx} and transverse MR curves. As mentioned above, the characteristic increase in ρ_{xx} with logarithmic temperature dependence below 20 K in the amorphous $Co_{0.61}Si_{0.39}$ film (see Figure 3e) can be explained in terms of the Kondo effect due to the coupling of electrons with localized magnetic impurities. The Kondo effect is not expected to occur in ferromagnetic materials,[62] thus explaining why there is no low-temperature upturn in ρ_{xx} in the case of textured $Co_{0.60}Si_{0.40}$ films (see Figure 3a). Moreover, the negative transverse MR occurring in the textured $Co_{0.60}Si_{0.40}$ film (see Figure 4a) is consistent with the presence of robust ferromagnetic interactions and consequent reduction in spin-flip scattering;[63,64] yet, a small hint of negative transverse MR is actually also visible in the amorphous $Co_{0.61}Si_{0.39}$ film at low temperature and magnetic field (see Figure S10).

To make a comparison of our magnetization data with literature, we mention that CoSi single crystals are diamagnetic at a temperature as low as 20 K, below which paramagnetism may occur due to the contribution of paramagnetic centers generated by self-doping effects.[19] Nonetheless, a quantum-phase transition from Pauli paramagnetism to a magnetically ordered state was found in polycrystalline $Co_{1-x}Si_x$ ribbons above a critical cobalt excess of about 2.9%.[22] Besides, room-temperature skyrmions were identified after thinning down the samples to about 50 nm by means of focused ion beam milling. Moreover, it has been suggested that surface ferromagnetism may emerge in nominally diamagnetic CoSi flakes, possibly due to the presence of distorted bonds and ordered vacancies near the sample surface.[30] Our results on magnetic characterization unambiguously demonstrate that structural and chemical disorder brings about signatures of magnetic ordering not only in Co-rich $Co_{1-x}Si_x$ films but also in the nearly stoichiometric $Co_{1-x}Si_x$ samples within a range of $x \approx \pm 3\%$ (i.e., not only for Co, but also for Si excess) and even in the case of amorphous $Co_{1-x}Si_x$ films with only a 1% Si excess. The latter is particularly relevant, because in general from an experimental perspective the control of the stoichiometry of thin films with an accuracy better than 1% using conventional thin films deposition methods poses a serious challenge.

Hall Effect Analysis. We shall now focus on the results of the Hall effect analysis of amorphous and textured $Co_{1-x}Si_x$ films at different temperatures and applied magnetic fields (see Figure 6). The antisymmetrized Hall resistivity ρ_{xy} of textured $Co_{1-x}Si_x$ films in the range of $0.4 < x < 0.6$ is characterized by a linear, negative slope, i.e., a negative Hall coefficient R_H, with the only exception being the textured $Co_{0.60}Si_{0.40}$ film at fields below 1 T. The predominance of a negative sign of R_H strongly indicates that electrons are the main charge carriers contributing to the electrical transport properties.

The Hall response of amorphous $Co_{1-x}Si_x$ films is somewhat more complex and displays different regimes. In the case of the amorphous $Co_{0.61}Si_{0.39}$ film, ρ_{xy} reveals initially a steep positive response for fields below 0.7 T, followed by a pronounced kink with nearly saturation of the Hall signal. The amorphous $Co_{1-x}Si_x$ samples with $x = 0.47$ and 0.51 present a transition from positive to negative Hall coefficient at about 1 T, followed by linear ρ_{xy} at high fields, whereas a negative, quasi-linear Hall response prevails for the amorphous $Co_{0.43}Si_{0.57}$ film.

At first glance, the transition from low-field, positive to high-field, negative Hall coefficients occurring in some of our $Co_{1-x}Si_x$ thin films may suggest a crossover from hole- to electron-dominated transport regimes. A nonlinear Hall response with reversal of its sign is not uncommon in semimetals, and often a two-band Hall model is employed to fit ρ_{xx} and ρ_{xy} curves in order to extrapolate the charge carrier density and mobility of holes and electrons pockets.[65,66] However, as explained in another work[67] and akin to the situation of our $Co_{1-x}Si_x$ thin films, in the presence of quasi-linear MR the condition on ρ_{xx} cannot be fit to the standard two-carrier model, as the linear component is not described by it.

The interpretation of the Hall effect data is further entangled by the presence of magnetism in our $Co_{1-x}Si_x$ thin films. Indeed, reversal of the sign of the Hall coefficient from positive to negative upon increasing the applied magnetic field is known in polycrystalline films of cobalt[68,69] and also amorphous, Co-based alloys[70] owing to the different contributions of anomalous and ordinary Hall effects. The former provides a positive (similar to holes), low-field Hall signal until magnetic saturation is reached; at larger fields the Hall coefficient turns negative, because only the ordinary Hall component associated with electrons concurs to the transport. Given the presence of magnetic ordering in our $Co_{1-x}Si_x$ thin films (particularly for the Co-rich samples), it is not too surprising that some of our CoSi films display an anomalous Hall effect at low magnetic fields. A tentative analysis of the anomalous Hall effect in amorphous $Co_{0.61}Si_{0.39}$ films with the aim to distinguish between the intrinsic mechanism caused by Berry curvature and extrinsic skew scattering and side-jump mechanisms is proposed in the Supporting Information (Figure S15).

Regardless of the low-field, nonlinear Hall response displayed by some of our $Co_{1-x}Si_x$ thin films, the high-field Hall resistivity of *all* $Co_{1-x}Si_x$ samples is linear and negative (with the amorphous $Co_{0.61}Si_{0.39}$ film as the only exception). First, the negative slope provides a strong indication that electrons are the charge carriers dominating the magnetotransport properties. Second, the linear character of ρ_{xy} at high fields motivates the use—in first approximation—of a single-carrier Drude band model to estimate the charge carrier density n and the Hall mobility μ_H of electrons according to the relations $\rho_{xy} = R_H \cdot B = \frac{1}{nq}$ (with R_H as the Hall coefficient and $q \approx 1.602 \times 10^{19}$ C the elementary charge) and $\rho_{xx} = \frac{R_H}{\mu_H}$.

https://doi.org/10.1021/acsaelm.3c00095
ACS Appl. Electron. Mater. 2023, 5, 2624−2637

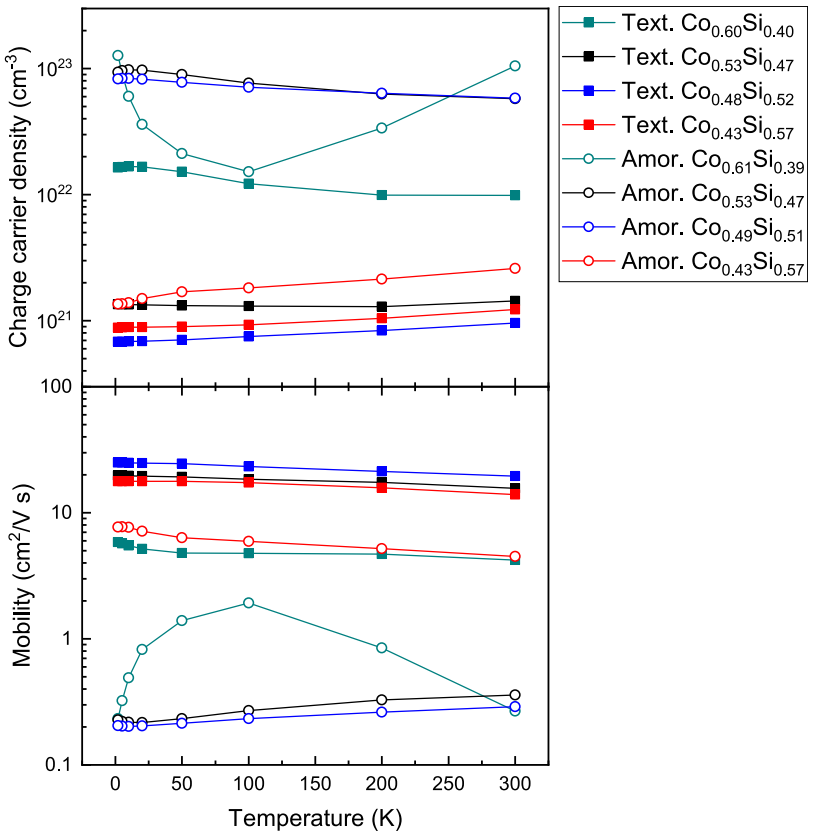

Figure 7. Charge carrier density (top) and Hall mobility (bottom) of amorphous (empty symbols) and textured (filled symbols) $Co_{1-x}Si_x$ films extracted from the high-field (>2 T) Hall resistivity data using a single-carrier band model.

Notably, a one-band model was used to interpret Hall effect data also in the case of single crystals of the topological Weyl semimetal NbP displaying nonlinear Hall behavior at low magnetic fields.[71]

The charge carrier density and Hall mobility of amorphous and textured $Co_{1-x}Si_x$ thin films are plotted as a function of temperature in Figure 7. No abrupt variations in n or μ_H with temperature were found, with the only exception of the amorphous $Co_{0.61}Si_{0.39}$ film.

According to a one-band model, textured $Co_{1-x}Si_x$ films have a maximum $n \approx 1 \times 10^{22}$ cm^{-3} for $x = 0.40$, whereas for the other compositions n drops to 10^{20-21} cm^{-3}. The tendency toward lower values of charge carrier density upon increasing the Si content is another indication of the aforementioned evolution from metallic to semiconducting-like behavior in $Co_{1-x}Si_x$ films. The charge carrier density of the textured $Co_{0.48}Si_{0.52}$ film, virtually the one resembling most the condition of crystalline, stoichiometric CoSi, is about $n \approx 7 \times 10^{20}$ cm^{-3} at 2 K, which is slightly higher than the values of $(1-3) \times 10^{20}$ cm^{-3} reported for stoichiometric CoSi single crystals.[17] Notably, the amorphous $Co_{1-x}Si_x$ samples in the range $0.39 < x < 0.51$ feature an electron carrier density of $n \approx 1 \times 10^{23}$ cm^{-3}, which is about 1 to 2 orders of magnitude higher than in textured $Co_{1-x}Si_x$ films. Such large values of charge carrier densities are more consistent with metallic rather than semimetallic behavior, which could be explained by the large amount of disorder-induced states dramatically increasing the density of states (DOS) of the semimetal. Furthermore, when the silicon content is increased to $x = 0.57$ in amorphous $Co_{1-x}Si_x$ the charge carrier density drops by nearly 2 orders of magnitude. Taken together, the drop in charge carrier density and the change in carrier type to full electron-like as a function of x could be interpreted as a transition through a band touching point, crossed upon silicon doping the cobalt bands at the Fermi energy.[72]

An evident effect of the film microstructure is that textured $Co_{1-x}Si_x$ films present a Hall mobility on the order of $\mu_H \approx 20$ cm^2/V s, which is nearly 2 orders of magnitude larger than in the case of amorphous $Co_{1-x}Si_x$ films having $\mu_H \approx 0.22$ cm^2/V s. As expected, both amorphous and textured $Co_{1-x}Si_x$ films feature lower values of Hall mobilities as compared to CoSi single crystals[17] ($\mu_H \approx 230-7300$ cm^2/V s). We note that the amorphous $Co_{0.43}Si_{0.57}$ film presents a higher mobility $\mu_H \approx 7.5$ cm^2/V s at 2 K as compared to the other amorphous samples. Typically, Hall mobilities in amorphous materials are close to about 0.1 cm^2/V s with relatively little sensitivity to structural and compositional variations.[73] The seeming discrepancy in the mobility of the amorphous $Co_{0.43}Si_{0.57}$ film is possibly another manifestation of EEI, which, differently from localization effects, can cause an increase in the Hall coefficient.[55,74]

After extracting the values of n and μ_H with a one-band model, it becomes clearer why the resistivities of amorphous $Co_{1-x}Si_x$ films are comparable to textured $Co_{1-x}Si_x$ films regardless of their very different microstructures (see Figure 3). Considering $\rho_{xx} = (nq\mu_H)^{-1}$, the lower Hall mobilities of amorphous $Co_{1-x}Si_x$ films are compensated by their larger values of charge carrier densities.

After completing the surveys on the magnetotransport and magnetic properties on amorphous and textured $Co_{1-x}Si_x$ films, we shall now shed some light on the change in sign and the crossover from parabolic to quasi-linear observed in the MR results.

https://doi.org/10.1021/acsaelm.3c00095
ACS Appl. Electron. Mater. 2023, 5, 2624−2637

Several mechanisms, comprising quantum MR,[75] conductivity fluctuations,[67,76] and quantum electron−electron interference,[62] can induce nonsaturating, quasi-linear positive transverse MR in metals and semimetals.

Quantum MR implies the charge carriers to be in the quantum limit and occupy the lowest Landau level according to the condition $n_e \ll \left(\frac{2\pi eH}{hc}\right)^{3/2}$ (with n the charge carrier density, H the magnetic field, c the speed of light, and h the Planck constant). Our $Co_{1-x}Si_x$ films do not fulfill this condition, because a charge carrier density $n_e \approx 10^{21-23}$ cm^{-3} would require much larger values of magnetic fields as compared to the crossover field B_L of about 1−2 T, above which a transition from parabolic to quasi-linear transverse MR is observed.[75]

Conductivity fluctuations take place in inhomogeneous conductors with macroscopic spatial fluctuations in carrier density and/or mobility. In these circumstances charge carriers may scatter with low-mobility islands, thus causing the electrical current to deviate from the direction of the applied electric field E due to the emergence of a Hall component perpendicular to both E and B. Such an additional Hall contribution is responsible for the onset of linear, nonsaturating MR response. Given the large intrinsic disorder of our $Co_{1-x}Si_x$ films, it is tempting to invoke conductivity fluctuations as a possible mechanism for the observed quasi-linear MR response. One of the fingerprints of conductivity fluctuations is that sizable differences in mobility and charge carrier density take place upon the crossover from quadratic to quasi-linear regimes.[67] As mentioned, at high temperature the transverse MR curves of our $Co_{1-x}Si_x$ films can be well described with a parabolic dependence as a function of the applied magnetic field, whereas below 50 K the transverse MR curves undergo a crossover to a quasi-linear response. However, as can be seen from Figure 7, the values of charge carrier density and mobility of our $Co_{1-x}Si_x$ films vary smoothly throughout the whole investigated temperature range (apart from the amorphous $Co_{0.43}Si_{0.57}$ film). Besides, another feature of conductivity fluctuations is that when the orientation of the magnetic field is turned from perpendicular to parallel with respect to the direction of the current flow, the magnitude of the transverse MR decreases and, depending on the film thickness, can even turn from positive to negative.[77] As a matter of fact, conductivity fluctuations are one of the possible phenomena, such as also chiral anomaly or current jetting, that can give rise to negative longitudinal MR in topological semimetals. However, there is a quite good overlap between the transverse and longitudinal MR curves in our $Co_{1-x}Si_x$ films, thus indicating a rather isotropic MR response upon modification of the orientation of the magnetic field (see Figure S11). For these reasons, this effect alone cannot adequately explain our MR results.

In an alternative scenario, the unusual MR may be correlated to the intrinsic magnetism of our $Co_{1-x}Si_x$ films. Ferromagnetic materials typically exhibit negative MR owing to the strong spin−orbit coupling suppressing spin-flip interband scattering of electrons.[63,64] This explanation is compatible with the negative MR observed in the textured $Co_{0.60}Si_{0.40}$ film at low temperature and magnetic fields (see Figure 4a), which is also the sample with the most prominent ferromagnetic signal in terms of both M_s and H_c. Nonetheless, the dominant transverse MR response of $Co_{1-x}Si_x$ thin films is positive with a transition from parabolic to quasi-linear MR at low temperature upon increasing the magnetic field. In this respect, we notice that linear and positive MR is not unusual in disordered ferromagnetic systems such as $Fe_{1-y}Co_ySi$ and thin films of Fe, Ni, Co, and their granular mixtures with nonmagnetic materials as a consequence of quantum corrections to the conductivity due to EEI.[62,78] The positive and linear MR generated by EEI is typically isotropic with respect to the applied magnetic field and can occur at temperatures as high as 100 K. These two features indicate that quantum corrections to conductivity due to EEI remain a plausible scenario for the explanation of the linear and positive MR observed in our $Co_{1-x}Si_x$ films.

CONCLUSIONS

In summary, this work reveals the strong correlation between microstructure, chemical composition, magnetotransport, and magnetic properties in ≈25 nm $Co_{1-x}Si_x$ thin films with $0.40 < x < 0.60$. Both amorphous and textured $Co_{1-x}Si_x$ thin films undergo a progressive transition from metallic to semiconducting-like conduction regimes upon increasing the silicon content. Most importantly, the values of resistivities are on the same order of magnitude independently of the film microstructure; this is quite unexpected since electrical conduction is heavily hampered in conventional disordered materials as compared to their crystalline counterparts. A possible reason comes from the results of one-band Hall effect analysis: amorphous $Co_{1-x}Si_x$ thin films have a lower mobility, but also a higher charge carrier concentration than textured $Co_{1-x}Si_x$ thin films, likely resulting from a disorder-enhanced DOS in the semimetallic region which almost entirely compensates for the much lower carrier mobilities. Other factors possibly contributing to the increase of carrier density include the presence of dangling bonds[79] and topological surface states. The latter find support in a recent theoretical work[36] reporting that amorphous metals can host exotic topological phases despite the lack of long-range translational symmetry. Our findings, notably the semimetallic nature of the $Co_{1-x}Si_x$ samples, the abrupt drop in charge carrier density, and the change of carrier type to full electron-like as a function of x, are consistent with the survival of band touchings with low density of states. We also note that some of the transport anomalies, such as EEI and localization effects, observed in our $Co_{1-x}Si_x$ films have also been reported in other studies on thin films of the topological semimetal Cd_3As_2 and the topological insulator Bi_2Se_3.[41,42] However, discerning whether topological features survive structural disorder and what is their potential correlation with transport anomalies (e.g., Kondo, WL, EEI, and anomalous Hall effects) requires developing models for amorphous and textured CoSi, currently unavailable. Experimentally, a promising strategy to evaluate the possible occurrence of topological surface states in amorphous and textured $Co_{1-x}Si_x$ films would be to analyze the scaling behavior of the film resistivity as compared to conventional materials upon reducing the film thickness.

The MR of $Co_{1-x}Si_x$ films displays a variety of responses, such as sign reversal and transition from quadratic to quasi-linear regimes, which can be ascribed to quantum corrections due to EEI. All the $Co_{1-x}Si_x$ films present signatures of magnetic exchange interactions, whose strength is directly correlated to the amount and distribution of cobalt, even in the case of nearly stoichiometric $Co_{1-x}Si_x$ films. This result poses a challenge concerning the realization of $Co_{1-x}Si_x$ films with transport, magnetic, and topological characteristic similar to

https://doi.org/10.1021/acsaelm.3c00095
ACS Appl. Electron. Mater. 2023, 5, 2624−2637

CoSi bulk single crystal. On the other hand, a careful adjustment of the concentration and size of magnetic centers in low-dimensional $Co_{1-x}Si_x$ films may also offer new degrees of freedom to tailor the properties of CoSi beyond bulk systems.

In conclusion this work will serve as a valuable case study to pinpoint the sensitivity of low-dimensional $Co_{1-x}Si_x$ thin films with respect to structural and chemical disorder and to critically evaluate the potential implementation of the chiral semimetal CoSi in nanoscale thin films and topological devices.

EXPERIMENTAL SECTION

Thin Film Growth and Characterization. Prior to insertion in vacuum (001)-oriented, epi-polished MgO substrates (size 10 mm × 10 mm × 1 mm) were ultrasonically cleaned for 5 min in isopropyl alcohol. After that, the MgO substrates were outgassed at about 450 °C for 30 min under ultra-high-vacuum conditions. The base pressure of the MBE system was around 10^{-10} mbar, which increased to 10^{-9}–10^{-8} mbar during film growth. Co and Si elements were deposited from electron-beam sources at a deposition rate of ≈0.1 Å/s. The Co and Si fluxes were calibrated prior to MBE deposition via a quartz crystal microbalance and maintained constant during MBE deposition using quadrupole mass spectrometers coupled to the electron-beam sources. $Co_{1-x}Si_x$ thin films were deposited following a layer-by-layer growth process by opening/closing the metal shutters in front of the electron-beam sources. The MBE growth temperature was monitored via a type K thermocouple after calibration with a pyrometer.

After MBE growth the structural characterization of the $Co_{1-x}Si_x$ thin films have been done via atomic force microscopy, grazing-incident X-ray diffraction, synchrotron pole figures, and scanning transmission electron microscopy. The preparation of cross sectional lamellas was done by means of focused ion beam (FIB) milling; to mitigate the damage induced by FIB preparation, a protective Al_2O_3 layer (about 40 nm) grown by atomic layer deposition was added onto the $Co_{1-x}Si_x$ films. For chemical characterization Rutherford backscattering spectroscopy, energy dispersive X-ray analysis, and X-ray photoelectron spectroscopy were employed. Additional details can be found in the Supporting Information.

Magnetotransport and Magnetization Measurements. The original $Co_{1-x}Si_x$ thin films grown on a MgO substrate were sliced into Hall bars with a size of about 10 mm × 1.5 mm × 1 mm (length, width, thickness) using a diamond cut tool. Metallic contacts for 4-point probe resistance and Hall effect measurements were prepared via wire bonding. The current leads were covered with silver paste in order to provide better uniformity of the current flow. The input current was set to 0.05 mA. The resistivity, MR, Hall effect, and magnetization of $Co_{1-x}Si_x$ thin films were characterized via a physical properties measurement system (PPMS) in the range of 2−300 K and applied magnetic fields up to ±9 T. The analysis of the Hall effect data was carried out after removal of the symmetric Hall contribution due to the misalignment of the voltage probes.

ASSOCIATED CONTENT

Supporting Information

The Supporting Information is available free of charge at https://pubs.acs.org/doi/10.1021/acsaelm.3c00095.

AFM images at different growth temperatures, XRD and pole figure analysis, RBS analysis, XPS analysis, STEM analysis, Hall bar size and measurement configuration, low-temperature resistivity fits, analysis of Mooij correlations, low-field transverse MR in amorphous and textured $Co_{1-x}Si_x$ films, resistivity fit of amorphous $Co_{0.43}Si_{0.57}$ films with and without magnetic field, derivative of the transverse MR, longitudinal MR analysis, magnetic characterization at different temperatures, analysis of anomalous Hall effect in amorphous $Co_{0.61}Si_{0.39}$ films (PDF)

AUTHOR INFORMATION

Corresponding Authors

Alan Molinari − *IBM Research Europe − Zurich, 8803 Rüschlikon, Switzerland;* orcid.org/0000-0001-6408-6446; Email: molinarialan86@gmail.com

Heinz Schmid − *IBM Research Europe − Zurich, 8803 Rüschlikon, Switzerland;* orcid.org/0000-0002-0228-4268; Email: sih@zurich.ibm.com

Authors

Federico Balduini − *IBM Research Europe − Zurich, 8803 Rüschlikon, Switzerland*

Lorenzo Rocchino − *IBM Research Europe − Zurich, 8803 Rüschlikon, Switzerland*

Rafał Wawrzyńczak − *Max Planck Institute for Chemical Physics of Solids, 01187 Dresden, Germany*

Marilyne Sousa − *IBM Research Europe − Zurich, 8803 Rüschlikon, Switzerland*

Holt Bui − *IBM Research-Almaden Research Center, San Jose, California 95120, United States*

Christian Lavoie − *IBM T.J. Watson Research Center−38-251, Yorktown Heights, New York 10598, United States*

Vesna Stanic − *IBM T.J. Watson Research Center−38-251, Yorktown Heights, New York 10598, United States*

Jean Jordan-Sweet − *IBM T.J. Watson Research Center−38-251, Yorktown Heights, New York 10598, United States*

Marinus Hopstaken − *IBM T.J. Watson Research Center−38-251, Yorktown Heights, New York 10598, United States*

Serguei Tchoumakov − *Université Grenoble Alpes, CNRS, Grenoble INP, Institut Néel, 38000 Grenoble, France*

Selma Franca − *Université Grenoble Alpes, CNRS, Grenoble INP, Institut Néel, 38000 Grenoble, France*

Johannes Gooth − *Max Planck Institute for Chemical Physics of Solids, 01187 Dresden, Germany*

Simone Fratini − *Université Grenoble Alpes, CNRS, Grenoble INP, Institut Néel, 38000 Grenoble, France*

Adolfo G. Grushin − *Université Grenoble Alpes, CNRS, Grenoble INP, Institut Néel, 38000 Grenoble, France*

Cezar Zota − *IBM Research Europe − Zurich, 8803 Rüschlikon, Switzerland*

Bernd Gotsmann − *IBM Research Europe − Zurich, 8803 Rüschlikon, Switzerland;* orcid.org/0000-0001-8978-7468

Complete contact information is available at: https://pubs.acs.org/10.1021/acsaelm.3c00095

Notes

The authors declare no competing financial interest.

ACKNOWLEDGMENTS

The authors acknowledge Ching-Tzu Chen, Jean Fompeyrine, Philip Moll, Kirsten Moselund, Heinz Siegwart, Victor Andre Meynier, Daniele Caimi, and John Bruley for fruitful discussions and technical support. This project has received funding from the European Union's Horizon 2020 research and innovation program under the Marie Sklodowska-Curie grant agreement No. 898113 (InNaTo) and the grant agreement No. 829044 (SCHINES). We thank the Cleanroom Operations Team of the Binning and Rohrer Nanotechnology

Center (BRNC) for their help and support. Part of this research used NIST beamline 6-BM of the National Synchrotron Light Source II, a U.S. Department of Energy (DOE) Office of Science User Facility operated for the DOE Office of Science by Brookhaven National Laboratory under Contract No. DE-SC0012704.

REFERENCES

(1) Liang, T.; Gibson, Q.; Ali, M. N.; Liu, M.; Cava, R. J.; Ong, N. P. Ultrahigh Mobility and Giant Magnetoresistance in the Dirac Semimetal Cd_3As_2. *Nat. Mater.* **2015**, *14* (3), 280−284.

(2) Kumar, N.; Sun, Y.; Xu, N.; Manna, K.; Yao, M.; Süss, V.; Leermakers, I.; Young, O.; Förster, T.; Schmidt, M.; Borrmann, H.; Yan, B.; Zeitler, U.; Shi, M.; Felser, C.; Shekhar, C. Extremely High Magnetoresistance and Conductivity in the Type-II Weyl Semimetals WP_2 and MoP_2. *Nat. Commun.* **2017**, *8* (1), 1−8.

(3) Ma, J.; Gu, Q.; Liu, Y.; Lai, J.; Yu, P.; Zhuo, X.; Liu, Z.; Chen, J. H.; Feng, J.; Sun, D. Nonlinear Photoresponse of Type-II Weyl Semimetals. *Nat. Mater.* **2019**, *18* (5), 476−481.

(4) Han, F.; Andrejevic, N.; Nguyen, T.; Kozii, V.; Nguyen, Q. T.; Hogan, T.; Ding, Z.; Pablo-Pedro, R.; Parjan, S.; Skinner, B.; Alatas, A.; Alp, E.; Chi, S.; Fernandez-Baca, J.; Huang, S.; Fu, L.; Li, M. Quantized Thermoelectric Hall Effect Induces Giant Power Factor in a Topological Semimetal. *Nat. Commun.* **2020**, *11* (1), 6167.

(5) Gooth, J.; Schierning, G.; Felser, C.; Nielsch, K. Quantum Materials for Thermoelectricity. *MRS Bull.* **2018**, *43* (3), 187−192.

(6) Ni, Z.; Wang, K.; Zhang, Y.; Pozo, O.; Xu, B.; Han, X.; Manna, K.; Paglione, J.; Felser, C.; Grushin, A. G.; de Juan, F.; Mele, E. J.; Wu, L. Giant Topological Longitudinal Circular Photo-Galvanic Effect in the Chiral Multifold Semimetal CoSi. *Nat. Commun.* **2021**, *12* (1), 1−8.

(7) Parameswaran, S. A.; Grover, T.; Abanin, D. A.; Pesin, D. A.; Vishwanath, A. Probing the Chiral Anomaly with Nonlocal Transport in Three-Dimensional Topological Semimetals. *Phys. Rev. X* **2014**, *4* (3), 1−12.

(8) Tang, S.; Zhang, C.; Wong, Di.; Pedramrazi, Z.; Tsai, H. Z.; Jia, C.; Moritz, B.; Claassen, M.; Ryu, H.; Kahn, S.; Jiang, J.; Yan, H.; Hashimoto, M.; Lu, D.; Moore, R. G.; Hwang, C. C.; Hwang, C.; Hussain, Z.; Chen, Y.; Ugeda, M. M.; Liu, Z.; Xie, X.; Devereaux, T. P.; Crommie, M. F.; Mo, S. K.; Shen, Z. X. Quantum Spin Hall State in Monolayer 1T′-WTe_2. *Nat. Phys.* **2017**, *13* (7), 683−687.

(9) Bulmash, D.; Qi, X. L. Quantum Oscillations in Weyl and Dirac Semimetal Ultrathin Films. *Phys. Rev. B* **2016**, *93* (8), 1−5.

(10) Yang, K. Y.; Lu, Y. M.; Ran, Y. Quantum Hall Effects in a Weyl Semimetal: Possible Application in Pyrochlore Iridates. *Phys. Rev. B - Condens. Matter Mater. Phys.* **2011**, *84* (7), 12−18.

(11) Krishna Nichenametla, C.; Calvo, J.; Riedel, S.; Gerlich, L.; Hindenberg, M.; Novikov, S.; Burkov, A.; Kozelj, P.; Cardoso-Gil, R.; Wagner-Reetz, M. Doping Effects in CMOS-Compatible CoSi Thin Films for Thermoelectric and Sensor Applications. *Zeitschrift fur Anorg. und Allg. Chemie* **2020**, *646* (14), 1231−1237.

(12) Rembieliński, J.; Caban, P. Relativistic Chiral Qubits, Their Time Evolution, and Correlations. *Phys. Rev. A* **2019**, *99* (2), No. 022320.

(13) Rajamathi, C. R.; Gupta, U.; Kumar, N.; Yang, H.; Sun, Y.; Süß, V.; Shekhar, C.; Schmidt, M.; Blumtritt, H.; Werner, P.; Yan, B.; Parkin, S.; Felser, C.; Rao, C. N. R. Weyl Semimetals as Hydrogen Evolution Catalysts. *Adv. Mater.* **2017**, *29* (19), 1−6.

(14) Sanchez, D. S.; Belopolski, I.; Cochran, T. A.; Xu, X.; Yin, J. X.; Chang, G.; Xie, W.; Manna, K.; Süß, V.; Huang, C. Y.; Alidoust, N.; Multer, D.; Zhang, S. S.; Shumiya, N.; Wang, X.; Wang, G. Q.; Chang, T. R.; Felser, C.; Xu, S. Y.; Jia, S.; Lin, H.; Hasan, M. Z. Topological Chiral Crystals with Helicoid-Arc Quantum States. *Nature* **2019**, *567* (7749), 500−505.

(15) Rao, Z.; Li, H.; Zhang, T.; Tian, S.; Li, C.; Fu, B.; Tang, C.; Wang, L.; Li, Z.; Fan, W.; Li, J.; Huang, Y.; Liu, Z.; Long, Y.; Fang, C.; Weng, H.; Shi, Y.; Lei, H.; Sun, Y.; Qian, T.; Ding, H. Observation of Unconventional Chiral Fermions with Long Fermi Arcs in CoSi. *Nature* **2019**, *567* (7749), 496−499.

(16) Guo, C.; Hu, L.; Putzke, C.; Diaz, J.; Huang, X.; Manna, K.; Fan, F. R.; Shekhar, C.; Sun, Y.; Felser, C.; Liu, C.; Bernevig, B. A.; Moll, P. J. W. Quasi-Symmetry-Protected Topology in a Semi-Metal. *Nat. Phys.* **2022**, *18*, 813.

(17) Xu, X.; Wang, X.; Cochran, T. A.; Sanchez, D. S.; Chang, G.; Belopolski, I.; Wang, G.; Liu, Y.; Tien, H.; Gui, X.; Xie, W.; Hasan, M. Z.; Chang, T.; Jia, S. Crystal Growth and Quantum Oscillations in the Topological Chiral Semimetal CoSi. *Phys. Rev. B* **2019**, *100* (4), No. 045104.

(18) Wu, D. S.; Mi, Z. Y.; Li, Y. J.; Wu, W.; Li, P. L.; Song, Y. T.; Liu, G. T.; Li, G.; Luo, J. L. Single Crystal Growth and Magnetoresistivity of Topological Semimetal CoSi. *Chin. Phys. Lett.* **2019**, *36* (7), No. 077102.

(19) Stishov, S. M.; Petrova, A. E.; Sidorov, V. A.; Krasnorussky, V. N.; Menzel, D. Self-Doping Effects in Cobalt Silicide CoSi: Electrical, Magnetic, Elastic, and Thermodynamic Properties. *Phys. Rev. B - Condens. Matter Mater. Phys.* **2012**, *86* (6), 1−5.

(20) Burkov, A. T.; Novikov, S. V.; Zaitsev, V. K.; Reith, H. Transport Properties of Cobalt Monosilicide and Its Alloys at Low Temperatures. *Semiconductors* **2017**, *51* (6), 689−691.

(21) Adachi, K.; Ito, K.; Zhang, L.; Yamaguchi, M. Thermoelectric Properties of CoSi Thin Films. *Mater. Sci. Forum* **2003**, *426*−*432* (4), 3445−3450.

(22) Balasubramanian, B.; Manchanda, P.; Pahari, R.; Chen, Z.; Zhang, W.; Valloppilly, S. R.; Li, X.; Sarella, A.; Yue, L.; Ullah, A.; Dev, P.; Muller, D. A.; Skomski, R.; Hadjipanayis, G. C.; Sellmyer, D. J. Chiral Magnetism and High temperature Skyrmions in B20-Ordered Co-Si. *Phys. Rev. Lett.* **2020**, *124* (5), 57201.

(23) Seo, K.; Varadwaj, K. S. K.; Mohanty, P.; Lee, S.; Jo, Y.; Jung, M. H.; Kim, J.; Kim, B. Magnetic Properties of Single-Crystalline CoSi Nanowires. *Nano Lett.* **2007**, *7* (5), 1240−1245.

(24) Chen, C. T.; Bajpai, U.; Lanzillo, N. A.; Hsu, C. H.; Lin, H.; Liang, G. Topological Semimetals for Scaled Back-End-of-Line Interconnect beyond Cu. In *Technical Digest - International Electron Devices Meeting, IEDM*; 2020; Vol. *2020-Decem*, pp 32.4.1−32.4.4; DOI: 10.1109/IEDM13553.2020.9371996.

(25) Gall, D.; Cha, J. J.; Chen, Z.; Han, H. J.; Hinkle, C.; Robinson, J. A.; Sundararaman, R.; Torsi, R. Materials for Interconnects. *MRS Bull.* **2021**, *46* (10), 959−966.

(26) Lanzillo, N. A.; Bajpai, U.; Garate, I.; Chen, C.-T. Size-Dependent Grain Boundary Scattering in Topological Semimetals. 2022, 1−18; DOI: 10.48550/arXiv.2206.08214.

(27) Tu, K. N.; Ottaviani, G.; Thompson, R. D.; Mayer, J. W. Thermal Stability and Growth Kinetics of Co_2Si and CoSi in Thin-film Reactions. *J. Appl. Phys.* **1982**, *53* (6), 4406−4410.

(28) Okamoto, H. Co-Si (Cobalt-Silicon). *J. Phase Equilibria Diffus.* **2008**, *29* (3), 295−295.

(29) Liu, T. K.; Chiou, S. H.; Van Lierop, J.; Ouyang, C. Ab Initio Simulations of Defect-Based Magnetism: The Case of CoSi Nanowires. *RSC Adv.* **2016**, *6* (28), 23634−23639.

(30) Esin, V. D.; Timonina, A. V.; Kolesnikov, N. N.; Deviatov, E. V. Magnon Modes as a Joint Effect of Surface Ferromagnetism and Spin−Orbit Coupling in CoSi Chiral Topological Semimetal. *J. Magn. Magn. Mater.* **2021**, *540* (August), No. 168488.

(31) Armitage, N. P.; Mele, E. J.; Vishwanath, A. Weyl and Dirac Semimetals in Three-Dimensional Solids. *Rev. Mod. Phys.* **2018**, *90* (1), 15001.

(32) Xu, B.; Fang, Z.; Sánchez-Martínez, M. Á.; Venderbos, J. W. F.; Ni, Z.; Qiu, T.; Manna, K.; Wang, K.; Paglione, J.; Bernhard, C.; Felser, C.; Mele, E. J.; Grushin, A. G.; Rappe, A. M.; Wu, L. Optical Signatures of Multifold Fermions in the Chiral Topological Semimetal CoSi. *Proc. Natl. Acad. Sci. U. S. A.* **2020**, *117* (44), 27104−27110.

(33) Corbae, P.; Ciocys, S.; Varjas, D.; Kennedy, E.; Zeltmann, S.; Molina-Ruiz, M.; Griffin, S.; Jozwiak, C.; Chen, Z.; Wang, L.-W.; Minor, A. M.; Scott, M.; Grushin, A. G.; Lanzara, A.; Hellman, F. Evidence for Topological Surface States in Amorphous Bi_2Se_3. 2019, 1−40.

https://doi.org/10.1021/acsaelm.3c00095
ACS Appl. Electron. Mater. 2023, 5, 2624−2637

(34) Mitchell, N. P.; Nash, L. M.; Hexner, D.; Turner, A. M.; Irvine, W. T. M. Amorphous Topological Insulators Constructed from Random Point Sets. *Nat. Phys.* **2018**, *14* (4), 380−385.
(35) Agarwala, A.; Shenoy, V. B. Topological Insulators in Amorphous Systems. *Phys. Rev. Lett.* **2017**, *118* (23), 1−6.
(36) Yang, Y. B.; Qin, T.; Deng, D. L.; Duan, L. M.; Xu, Y. Topological Amorphous Metals. *Phys. Rev. Lett.* **2019**, *123* (7), 76401.
(37) Cheng, F.; Jiang, C.; Wu, J. Study of Crystallization and Phase Transformation in Amorphous Co-Si Thin Film by X-Ray Diffraction. *Mater. Trans.* **2004**, *45* (7), 2471−2473.
(38) Dulal, R. P.; Dahal, B. R.; Forbes, A.; Bhattarai, N.; Pegg, I. L.; Philip, J. Weak Localization and Small Anomalous Hall Conductivity in Ferromagnetic Weyl Semimetal Co_2TiGe. *Sci. Rep.* **2019**, *9* (1), 1−7.
(39) Jamer, M. E.; Assaf, B. A.; Devakul, T.; Heiman, D. Magnetic and Transport Properties of Mn_2CoAl Oriented Films. *Appl. Phys. Lett.* **2013**, *103* (14), 142403.
(40) Lin, C. P.; Hsu, C. Y.; Sun, S. J.; Chou, H. The Kondo Effect and Carrier Transport in Amorphous Cr-Doped In_2O_3 Thin Films. *AIP Adv.* **2012**, *2* (4), 042186.
(41) Zhao, B.; Cheng, P.; Pan, H.; Zhang, S.; Wang, B.; Wang, G.; Xiu, F.; Song, F. Weak Antilocalization in Cd_3As_2 Thin Films. *Sci. Rep.* **2016**, *6*, 1−7.
(42) Wang, J.; Dasilva, A. M.; Chang, C. Z.; He, K.; Jain, J. K.; Samarth, N.; Ma, X. C.; Xue, Q. K.; Chan, M. H. W. Evidence for Electron-Electron Interaction in Topological Insulator Thin Films. *Phys. Rev. B - Condens. Matter Mater. Phys.* **2011**, *83* (24), 1−7.
(43) Kazmerski, L. *Polycrystalline and Amorphous Thin Films and Devices*; Elsevier, 1980; DOI: 10.1016/B978-0-12-403880-6.X5001-3.
(44) Mott, N. F. Electrons in Disordered Structures. *Adv. Phys.* **1967**, *16* (61), 49−144.
(45) Mooij, J. H. Electrical Conduction in Concentrated Disordered Transition Metal Alloys. *Phys. Status Solidi* **1973**, *17*, 521−530.
(46) Lee, P. A.; Ramakrishnan, T. V. Disordered Electronic Systems. *Rev. Mod. Phys.* **1985**, *57*, 287−337.
(47) Tsuei, C. C. Nonuniversality of the Mooij Correlation − the Temperature Coefficient of Electrical Resistivity of Disordered Metals. *Phys. Rev. Lett.* **1986**, *57*, 1943−1946.
(48) Ciuchi, S.; Di Sante, D.; Dobrosavljević, V.; Fratini, S. The Origin of Mooij Correlations in Disordered Metals. *npj Quantum Mater.* **2018**, *3* (1), DOI: 10.1038/s41535-018-0119-y.
(49) Rademaker, L.; Fratini, S. Manuscript in Preparation, 2023.
(50) Sahu, P.; Fan, Y.; Peterson, T.; Chen, J.; Devaux, X.; Jaffrès, H.; Migot, S.; Dang, H.; George, J.; Lu, Y.; Wang, J. Room Temperature Mott Hopping and Spin Pumping Characterization of Amorphous Gd-Alloyed Bi_2Se_3. DOI: 10.48550/arXiv.1911.03323.
(51) Bahl, S. K.; Chopra, K. L. Amorphous versus Crystalline GeTe Films. III. Electrical Properties and Band Structure. *J. Appl. Phys.* **1970**, *41* (5), 2196−2212.
(52) Lu, H. Z.; Shen, S. Q. Quantum Transport in Topological Semimetals under Magnetic Fields. *Front. Phys.* **2017**, *12* (3), DOI: 10.1007/s11467-016-0609-y.
(53) Díaz, E.; Herrera, G.; Oyarzún, S.; Munoz, R. C. Evidence of Weak Anderson Localization Revealed by the Resistivity, Transverse Magnetoresistance and Hall Effect Measured on Thin Cu Films Deposited on Mica. *Sci. Rep.* **2021**, *11* (1), 1−11.
(54) Xie, Z.; Wei, X.; Cao, S.; Zhang, Y.; Yan, S.; Gu, G. D.; Li, Q.; Chen, J. H. Electron-Electron Interactions and Weak Antilocalization in Few-Layer $ZrTe_5$ Devices. *Phys. Rev. B* **2021**, *103* (15), 1−8.
(55) Bergmann, G. Weak Localization in Thin Films. *Phys. Rep.* **1984**, *107* (1), 1−58.
(56) Breznay, N. P.; Volker, H.; Palevski, A.; Mazzarello, R.; Kapitulnik, A.; Wuttig, M. Weak Antilocalization and Disorder-Enhanced Electron Interactions in Annealed Films of the Phase-Change Compound $GeSb_2Te_4$. *Phys. Rev. B - Condens. Matter Mater. Phys.* **2012**, *86* (20), 1−11.
(57) Brands, M.; Carl, A.; Posth, O.; Dumpich, G. Electron-Electron Interaction in Carbon-Coated Ferromagnetic Nanowires. *Phys. Rev. B - Condens. Matter Mater. Phys.* **2005**, *72* (8), 1−8.
(58) Sahnoune, A.; Strom-Olsen, J. O. Weak Localization and Enhanced Electron-Electron Interaction in Amorphous $Ca_{70}(Mg,Al)_{30}$. *Phys. Rev. B* **1989**, *39* (11), 7561−7566.
(59) Wang, W. J.; Gao, K. H.; Li, Z. Q. Thickness-Dependent Transport Channels in Topological Insulator Bi_2Se_3 Thin Films Grown by Magnetron Sputtering. *Sci. Rep.* **2016**, *6* (December 2015), 1−9.
(60) Venkatesan, M.; Kavle, P.; Porter, S. B.; Ackland, K.; Coey, J. M. D. Magnetic Analysis of Polar and Nonpolar Oxide Substrates. *IEEE Trans. Magn.* **2014**, *50* (11), 3−6.
(61) Bruvera, I. J.; Mendoza Zélis, P.; Pilar Calatayud, M.; Goya, G. F.; Sánchez, F. H. Determination of the Blocking Temperature of Magnetic Nanoparticles: The Good, the Bad, and the Ugly. *J. Appl. Phys.* **2015**, *118* (18), 184304.
(62) Gerber, A.; Kishon, I.; Korenblit, I. Y.; Riss, O.; Segal, A.; Karpovski, M.; Raquet, B. Linear Positive Magnetoresistance and Quantum Interference in Ferromagnetic Metals. *Phys. Rev. Lett.* **2007**, *99* (2), 1−4.
(63) Coey, J. M. D. *Magnetism and Magnetic Materials*; Cambridge University Press, 2010; Vol. 7, pp 181−185.
(64) Raquet, B.; Viret, M.; Sondergard, E.; Cespedes, O.; Mamy, R. Electron-Magnon Scattering and Magnetic Resistivity in 3d Ferromagnets. *Phys. Rev. B - Condens. Matter Mater. Phys.* **2002**, *66* (2), 244331−2443311.
(65) Jo, N. H.; Wu, Y.; Wang, L. L.; Orth, P. P.; Downing, S. S.; Manni, S.; Mou, D.; Johnson, D. D.; Kaminski, A.; Bud'Ko, S. L.; Canfield, P. C. Extremely Large Magnetoresistance and Kohler's Rule in $PdSn_4$: A Complete Study of Thermodynamic, Transport, and Band-Structure Properties. *Phys. Rev. B* **2017**, *96* (16), 1−13.
(66) Li, C. Z.; Li, J. G.; Wang, L. X.; Zhang, L.; Zhang, J. M.; Yu, D.; Liao, Z. M. Two-Carrier Transport Induced Hall Anomaly and Large Tunable Magnetoresistance in Dirac Semimetal Cd_3As_2 Nanoplates. *ACS Nano* **2016**, *10* (6), 6020−6028.
(67) Schumann, T.; Goyal, M.; Kealhofer, D. A.; Stemmer, S. Negative Magnetoresistance Due to Conductivity Fluctuations in Films of the Topological Semimetal Cd_3As_2. *Phys. Rev. B* **2017**, *95* (24), 1−6.
(68) Kötzler, J.; Gil, W. Anomalous Hall Resistivity of Cobalt Films: Evidence for the Intrinsic Spin-Orbit Effect. *Phys. Rev. B - Condens. Matter Mater. Phys.* **2005**, *72* (6), 1−4.
(69) Hou, D.; Li, Y.; Wei, D.; Tian, D.; Wu, L.; Jin, X. The Anomalous Hall Effect in Epitaxial Face-Centered-Cubic Cobalt Films. *J. Phys.: Condens. Matter* **2012**, *24* (48), 482001.
(70) Stobiecki, T.; Kossacki, P.; Szymczak, H. Sign Reversal of the Hall Coefficient in Amorphous Co-Zr Thin Films. *J. Magn. Magn. Mater.* **1991**, *101* (1−3), 211−212.
(71) Shekhar, C.; Nayak, A. K.; Sun, Y.; Schmidt, M.; Nicklas, M.; Leermakers, I.; Zeitler, U.; Skourski, Y.; Wosnitza, J.; Liu, Z.; Chen, Y.; Schnelle, W.; Borrmann, H.; Grin, Y.; Felser, C.; Yan, B. Extremely Large Magnetoresistance and Ultrahigh Mobility in the Topological Weyl Semimetal Candidate NbP. *Nat. Phys.* **2015**, *11* (8), 645−649.
(72) Sk, S.; Shahi, N.; Pandey, S. K. Experimental and Computational Approaches to Study the High Temperature Thermoelectric Properties of Novel Topological Semimetal CoSi. *J. Phys.: Condens. Matter* **2022**, *34*, 265901.
(73) Tauc, J. C. *Amorphous and Liquid Semiconductors*; Plenum Publishing Corporation, 1974; Chapter 5, pp 230−294.
(74) Yue, J.; Thoutam, L. R.; Prakash, A.; Wang, T.; Jalan, B. Unraveling the Effect of Electron-Electron Interaction on Electronic Transport in La-Doped $SrSnO_3$ Films. *Appl. Phys. Lett.* **2019**, *115* (8), 082102.
(75) Abrikosov, A. A. Quantum Linear Magnetoresistance; Solution of an Old Mystery. *J. Phys. A. Math. Gen.* **2003**, *36*, 9119−9131.
(76) Narayanan, A.; Watson, M. D.; Blake, S. F.; Bruyant, N.; Drigo, L.; Chen, Y. L.; Prabhakaran, D.; Yan, B.; Felser, C.; Kong, T.; Canfield, P. C.; Coldea, A. I. Linear Magnetoresistance Caused by Mobility Fluctuations in n -Doped Cd_3As_2. *Phys. Rev. Lett.* **2015**, *114* (11), 1−5.

(77) Hu, J.; Rosenbaum, T. F.; Betts, J. B. Current Jets Disorder, and Linear Magnetoresistance in the Silver Chalcogenides. *Phys. Rev. Lett.* **2005**, *95* (18), 1−4.
(78) Manyala, N.; Sidis, Y.; DiTusa, J. F.; Aeppli, G.; Young, D. P.; Fisk, Z. Magnetoresistance from Quantum Interference Effects in Ferromagnets. *Nature* **2000**, *408* (6812), 616−616.
(79) Hennig, R. G.; Fedders, P. A.; Carlsson, A. E. Electronic Structure of Dangling Bonds in Amorphous Silicon Studied via a Density-Matrix Functional Method. *Phys. Rev. B - Condens. Matter Mater. Phys.* **2002**, *66* (19), 1952131−1952136.

https://doi.org/10.1021/acsaelm.3c00095
ACS Appl. Electron. Mater. 2023, 5, 2624−2637